



POX - PANGU Optimization and eXperimental verification: design and performance

D. D'Urso^{1,2}, M. Duranti³, G. Ambrosi³, M. Barbanera^{3,7}, C. Brugnoli^{1,2*}, M. Caprai³, V. Formato⁴, E. Fiandrini^{5,3}, K. Kanxheri³, M. Ionica³, G. Silvestre^{5,3}, V. Scherini^{1,2**}, V. Sipala^{1,2}, and V. Vagelli^{6,3}

¹ Università di Sassari, I-07100 Sassari, Italy, e-mail: ddurso@uniss.it

² INFN - Laboratori Nazionali del Sud, I-95123 Catania, Italy

³ INFN - Sezione di Perugia, I-06100 Perugia, Italy, e-mail: matteo.duranti@infn.it

⁴ INFN - Sezione di Roma Tor Vergata, I-00133 Roma, Italy

⁵ Università degli Studi di Perugia, I-06100 Perugia, Italy

⁶ Agenzia Spaziale Italiana, I-00133 Roma, Italy

⁷ Università di Pisa, I-56122 Pisa, Italy

Received: 5 January 2022; Accepted: 5 June 2022

Abstract. Gamma-ray photons produced in the cosmos hold information about processes occurring in astrophysical sources as well as about fundamental physics. The Sub-GeV energy range, considered a crucial energy region to measure many astrophysical phenomena, is mostly unexplored. Several new ideas have been proposed to study gamma-ray photons in the MeV-GeV energy range, among them, the PAir-ProductioN Gamma-ray Unit (PANGU) [Wu et al. (2014)] project proposes the use of microstrip silicon detector technology, widely used in particle physics experiments, to improve the current angular resolution. In the current work, we present a detailed MC simulation of the detector, to assess the optimal silicon sensor thickness for the instrument, the construction of a working prototype of the optimal detector and the preparation of experimental setup to verify the point spread function of the optimized prototype with a tagged photon Beam Test.

Key words. Particle detector, silicon tracker, gamma-ray, cosmic rays

1. Introduction

Gamma-ray photons produced in the Cosmos provide information about processes occurring at astrophysical sources or open questions of fundamental physics, (e.g. the nature of Dark

Matter). Space-borne gamma-ray experiments and imaging air Cherenkov telescopes have discovered a variety of astrophysical sources and have brought new information on many high-energy astrophysics phenomena, mainly in the GeV energy region.

The Sub-GeV energy range, mostly unexplored, is considered a crucial energy region to measure many astrophysical phenomena.

* Now at Università degli Studi di Perugia

** Now at Università del Salento and INFN - Sez. di Lecce

Breaching the frontier of Sub-GeV gamma-rays will provide unprecedented and unique information on the origin and acceleration mechanism of high energy cosmic rays, the diffuse galactic gamma-ray background, the acceleration mechanisms of compact objects, the soft gamma-ray transients, the baryon asymmetry in the Early Universe, the Lorentz invariance, solar flares and terrestrial gamma-ray flashes, and on the electromagnetic counterparts of gravitational radiation and neutrinos. Furthermore, the Sub-GeV, is a suitable energy region where to search for gamma-ray lines which give possible hints of dark matter particle annihilation and/or decay (see [Funk (2015), Bykov et al. (2012), Rieger et al. (2013)] for a review about phenomena enlightened by gamma-ray astrophysics).

High angular resolution measurement is crucial to separate point source emission from the highly structured diffuse emission and to perform a reliable measurement of spectrum, point source identification and distribution. This represents, however, the most striking experimental challenge to explore the Sub-GeV region. Below ~ 10 MeV Compton scattering dominates the photon-nucleus cross-section, and the gamma-ray detection relies on the “production“ of a single electron out from the interaction of the incoming gamma-ray photons with the detector materials. At ~ 10 MeV, pair production become the dominant process of the photon-nucleus interaction, considering the scattering with low Z materials. On one hand, the small pair production cross section would require a detector with many radiation lengths to achieve the required acceptance. On the other hand, the amount of material would become the limiting factor of angular resolution due to the Multiple Coulomb Scattering (MCS). Under these conditions, a minimization of passive material, the use of a low density active detector and a large volume to assure an acceptable photon conversion rate is required to achieve an angular resolution that allows to resolve complex features of diffuse gamma-rays as well as to increase the point source sensitivity. In the years, several gamma-ray telescopes for photon-pair production detection, in this energy range, based on low den-

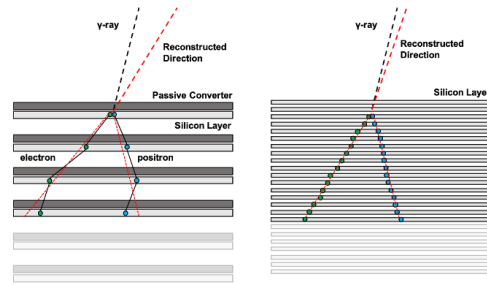


Fig. 1. Gamma-ray detection scheme in the GeV-TeV energy range (on the left) compared with PANGU detection idea (on the right): passive material has been removed and the thickness of active sensor layers has been reduced to minimize the MCS; number of silicon layers has been increased to recover pair-production efficiency.

sity gas Time Projection Chambers [Bernard et al. (2014), Hunter et al. (2014)], silicon detectors [Kanbach et al. (2005), Lebrun et al. (2010), O’Neill et al. (2001), Morselli et al. (2013)] and scintillating fibers [Pendleton et al. (1996), Pendleton et al. (1999)] have been proposed. In this document we discuss and provide a strategy for the experimental verification of the novel approach, that could enable the aforementioned revolution in the understanding of Sub-GeV gamma-rays, proposed for the PANGU detector.

2. The PANGU detection strategy to measure low energy gamma rays

The PAir-productionN Gamma-ray Unit (PANGU) [Wu et al. (2014)] project proposes the usage of silicon strip detector technology, with a novel approach, to build an instrument to go well beyond the sensitivity (i.e. angular resolution) of previous and current experiments. PANGU has been suggested as a candidate for the joint small mission between the European Space Agency (ESA) and the Chinese Academy of Science (CAS). The experimental approach is the same used at higher energies (GeV-TeV energy range): detect the gamma-ray photons through pair production (as, for example, in the Fermi-LAT [Atwood et al. (2009)] or DAMPE [Chang et al. (2017)] detectors) but adapting it to the lower energy,

where the MCS effect dominates and spoils the angular resolution. The heavy converter (i.e. tungsten) is removed, and a stack of tens of thinner tracking layers is used to recover the required detection efficiency (see Figure 1). The PANGU detection principle provides a superior photon pointing resolution in the Sub-GeV range. It may allow to measure also the polarization of gamma rays, opening a new frontier in gamma-ray astronomy. Furthermore, in one of the proposed PANGU layouts, the use of a spectrometric measurement, rather than on a calorimetric one, for the energy estimation of the impinging photon, is well suited for a small (100÷500 Kg) or even for a mini (10÷100 Kg) satellite mission.

3. POX: A possible approach for PANGU experimental verification

PANGU potentialities have been only estimated by Monte Carlo simulation. We propose a strategy to optimize the PANGU-like detector design, developing a detailed MC simulation of the tracking system, validating the MC studies by experimental data and constructing and assembling a new optimized tracking sensor. The strategy accomplished the following objectives/phases:

- development of a detailed MC simulation of the detector and a custom reconstruction software (SW), to study the optimal silicon sensor thickness for the instrument (see Sections 4 and 5);
- assembly of a working prototype of the optimal detector using the newly built tracking units (see Section 6);
- preparation of experimental setup to verify the point spread function of the optimized prototype with a tagged photon Beam Test, BT (see Section 7).

4. Detector simulation and layout

The POX [D'Urso (2017)] detector simulation has been developed using the GGS framework [Mori (2021)] interface to GEANT4 [Agostinelli *et al.* (2003)]. The detector geometry is completely configurable (number of

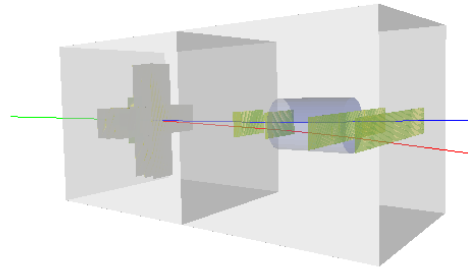


Fig. 2. One example of the layouts simulated in the MC simulation, a realistic 19-layers layout using also AMS and DAMPE space silicon sensors: converter/tracker section (left) and magnetic spectrometer one (right).

sensor tiles, dimensions, inter-layer distances etc.). The simulation chain includes signal digitization and realistic noise modelling. The reconstruction procedure implements custom algorithms for clustering, track finding and track fitting (see Section 5).

4.1. Detector layout

The detector layout, shown in one example in Figure 2, is generally constituted by a converter/tracker section, where photons can convert, and a magnetic spectrometer section, to estimate the energy of the e^-e^+ pairs and of parent photons, as foreseen by the PANGU layout (see Section 2). The sensor planes are aligned along the incident photon beam direction, that will be indicated as z axis. The vertical direction will be identified as the y axis, consequently the x axis will correspond to the perpendicular to the photon beam in the horizontal plane. The magnetic volume (blue in the figure) is a cylinder of length 20 cm, radius 7 cm and field 0.05 T. The magnetic field bending is placed the y axis.

The detector performance has been tested with different layer number, inter-layer distances, sensors thickness and readout parameters. For the silicon sensors, several sizes and thicknesses have been implemented in the simulation: AMS [Alpat *et al.* (2010)] and

DAMPE [Azzarello *et al.* (2016)] $\sim 300\mu\text{m}$ thick sensors with realistic supporting material (including epoxy-glue, Kapton foils, etc.), $50\times 50\text{ cm}^2$ “ideal” (to study the performances without facing edge problems) single-sided sensors and $9.5\times 9.5\text{ cm}^2$ single-sided “new” ones (similar to the ones actually built for the project, *cfr.* Section 6). The detector layout has been implemented in the following configurations for the systematic studies aimed at optimizing its performances:

- a) 14 “ideal” layers, thickness $300\mu\text{m}$, 10 for the tracker/converter section, spaced 3 cm, and 4 for the spectrometer section, spaced 10 cm (2 before and 2 after the magnetic field volume);
- b) 24 “ideal” layers, thickness $150\mu\text{m}$, 20 for converter and 4 for spectrometer, same dimensions, inter-layer spacing and magnetic volume as a);
- c) 19 layers in realistic configuration: 5 “new” sensors, thickness $150\mu\text{m}$, 9 AMS (4 in the spectrometric section) and 5 DAMPE ones, same inter-layer spacing and magnetic volume as a) and b) (see Figure 2);
- d) 24 layers in final configuration: 20 “new” sensors, thickness $150\mu\text{m}$, for the tracker/converter and 4 AMS layers for the spectrometer. Same inter-layer spacing and magnetic volumes as a), b) and c).

The configuration c) was designed for a BT, not possible due to the COVID-19 pandemic, to be performed with spare sensors and during the optimization phase, and with a first bunch of silicon sensors, maybe not with the final thickness. The configuration d), instead was the target final configuration that will be adopted for the BT campaign, with all the sensors built for the project.

Simulated pair-production events are shown, Figure 2, for the described exemplary detector configuration: left the incident photon track (green), right the emerging electron (red) and positron (blue) tracks.

Montecarlo output is processed by a tailored algorithm which mimics the digital readout of the silicon sensors, reproducing the Front-End electronics. The sensitive strips volumes are placed in the detector planes, alter-

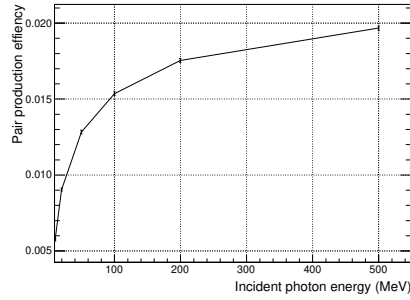


Fig. 3. Estimated pair-production efficiency in the converter/tracker section, for the layout a) described in Section 4.1.

nately oriented along the y or x axis, according to the implantation and readout pitches. The true signal is assigned to multiple adjacent strips following a realistic charge distribution while noise hits are modelled applying realistic noise components based on sensor measurements. The clustering algorithm, which has been already verified and used in test beams with similar instrumentation [Bigongiari *et al.* (2019); Dong *et al.* (2016)], performs the same decoding routines for Monte Carlo and BT data and delivers the event for the rest of the reconstruction.

4.2. Intrinsic detector performances

The detector performances have been evaluated in different detector configurations, at different energies and for different injected particles (protons, electrons, gammas).

Some performances, in particular the pair-production efficiency in the converter/tracker section, can be evaluated even before implementing a dedicated reconstruction software. The conversion efficiency has been estimated, as a function of energy (ranging from 10 to 500 MeV), with dedicated simulation runs of 10^6 injected photons for each energy and detector configuration. The obtained values range from $\leq 1\%$ to $\sim 2\%$, see Figure 3 for the layout a).

The Point Spread Function (PSF), main target study of the whole project, corresponds to the probability distribution function of the an-

gle between the expected and the reconstructed directions of the incoming gamma ray. It is often expressed in terms of width of the distribution containing the 68% of population. The PSF width is the result of the combined effect of angular uncertainties, due to the instrument intrinsic resolution, and the MCS. Details on expected values of the two effects, their combination and the angular resolution estimated for different gamma telescopes can be found in [Wu *et al.* (2014)] and [Hunter *et al.* (2014)].

The intrinsic effect of the MCS in the production layer can be estimated from simulations, again, even before applying the reconstruction SW. In Figure 4, top panel, the distribution of the space angle between the e^- and e^+ momenta directions at production and after traversing the production layer is plotted for an incident photon energy of 100 MeV. In Figure 4, bottom panel, the 68% containment angle is plotted as a function of the incident photon energy. The results are in agreement with the expectations of the PANGU collaboration [Wu *et al.* (2014)]. A gain of about 30% can be achieved by implementing the detector configuration b), confirming and quantifying the expectation for which thinner sensors can be used to mitigate the effect of MCS on the intrinsic PSF of the instrument.

5. Event reconstruction

Photon event reconstruction requires the identification of the positron/electron tracks recorded by the silicon detectors, the estimation of their momenta, of the photon conversion point and of the incident photon direction. To correctly identify pair tracks, the reconstruction algorithm should be able to distinguish signal and noise recorded hits. Noise hits can strongly affect the identification of the conversion point and the measurement of electron/positron momenta.

5.1. Event reconstruction strategy

In order to correctly point the incident photon direction, is necessary to reconstruct the directions and momenta of the electron-positron pair produced, also measuring the energy of the

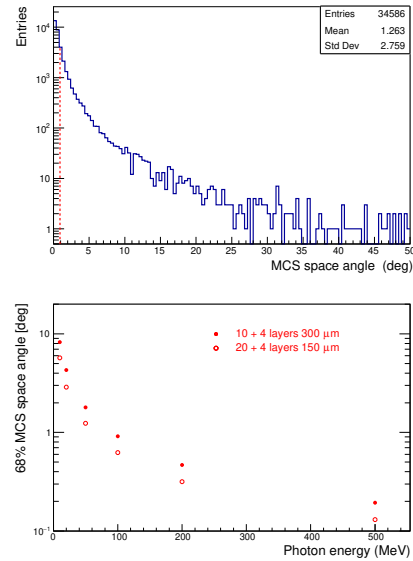


Fig. 4. Top panel: distribution of the angle between e^- and e^+ momenta at production and after the production layer for an incident photon with energy 100 MeV. Bottom panel: 68% of as a function of the incident photon energy. Filled circles configuration a), empty circles configuration b).

two distinct products, to combine them into the primary photon momentum.

Due to the intense multiple scattering of the low energy particles, the “tracks” are not straight and so a linear fit on the acquired clusters is not an effective way to determine with high accuracy the production angles for the pair particles. The strategy adopted to reconstruct the photon arrival direction is to only consider the first two layers after the conversion, for each view (x - z or y - z) of the tracker. Particle momentum is measured by means of a magnetic spectrometer thus it is mandatory to match the tracks stub out from the reconstructed vertex with those entering into the spectrometer. It is, thus, crucial to follow each track along its development.

The “vertex finding” and the “track reconstruction” are performed, indeed, with essentially two distinct approaches: the first one identifies the vertex, considering that only one of the two views can host it, the second tries to

identify all the clusters belonging to the track of a single particle. The matching of the two reconstructions, based on the spatial compatibility, is performed at the z position of the second or third layer after the vertex, and constitutes a goodness test for the overall reconstruction.

Vertex finding: given the low level of noise in the silicon sensors (cfr. Section 6.2), essentially the main issue, when identifying the vertex, is the “inefficiency” (a real energy deposit under-fluctuating, going under threshold and being considered a noisy hit) and the presence of the “vertex hit” only on one of the two views. The vertex is essentially identified by searching for a “triangle”, made ideally by 5 hits (even if holes are accepted), involving the most upward found layer with a single cluster and two layers with, ideally, two clusters each. Once this vertex is found, let's say in the x - z view, two track stubs involving the first following three layers (ideally 6 clusters) in the y - z view are selected. The crossing of these two stubs, linearly fitted, determines the coordinate (in this example on y) of the vertex on this view, once projected at the z of the layer (on the other view) of the vertex previously found. This completes the full vertex position: x , y and z . The directions identified from this vertex and the next pair of clusters, on the x and y views, are taken as the production directions of the two particles.

Track reconstruction: the strategy used is to perform a Hough Transform [Duda & Hart (1972)] on each view of the tracker (see [Mårtensson & the ATLAS Collaboration (2016)] for other example of Hough Transform application to the silicon tracker event reconstruction]). Generally, one of the two pair-produced particles is taking most part of the energy, so we expected to find two different kind of tracks, one much more regular than the other, due to the effect of MCS. Tracks are reconstructed iteratively, one by one, starting from the group of clusters with the maximum density in the parameter space. Then the procedure is repeated using clusters not yet associated to a track. In that way, straighter tracks are immediately identified and the corresponding clusters removed from the list of clusters to be associated. Consequently irregular tracks,

corresponding to the particle with less energy, are easier to be reconstructed and labelled.

In Figure 5 a few examples of reconstructed events are shown, as seen on the y - z view of the tracker, just as example. As expected, due to the low energy of the particles, the path can have sudden change of direction (central and right panels). If the pair production occurs in an x -oriented layer, for example, the tracks recorded by the y -oriented layers won't have a vertex (right panel), again as expected.

The whole track reconstruction is done in two completely independent processes for the two views of the tracker. This implies a degeneracy on the 3D event reconstruction: the $x - z$ view of the e^- can be wrongly combined with the $y - z$ of e^+ , and viceversa. This ambiguity is an issue when associating the momenta measurement with the production direction to point the source of the incident photon. The two views need to be recombined in the correct way. The matching with the vertex independently found, provides a possible mitigation of the problem, but the vertex finding algorithm is also exposed to this problem. The recovery of the degeneracy has been performed using a pair of x and y -oriented tilted layers at the end of the tracker/converter (see later).

5.2. Results

The developed custom reconstruction SW has allowed to evaluate, using MC simulated events, the performances of the detector in the different layouts. Similar results (for example for the reconstruction efficiencies) have been obtained for all the layouts. The numbers reported in the following and the PSF shown in Figures 7 and 8, have been obtained in the $150 \mu\text{m}$ thickness case, layout b).

Vertex finding: two coordinates out of three for the position of the production vertex can be determined with extreme precision. If the production occurs on a layer with strips along the x axis, the x and z coordinates are measured directly with an error of the order of tens of μm . The third coordinate is indeed inferred back projecting the positions of the hits from the next layers. The combination of the two independent measurements provides a result-

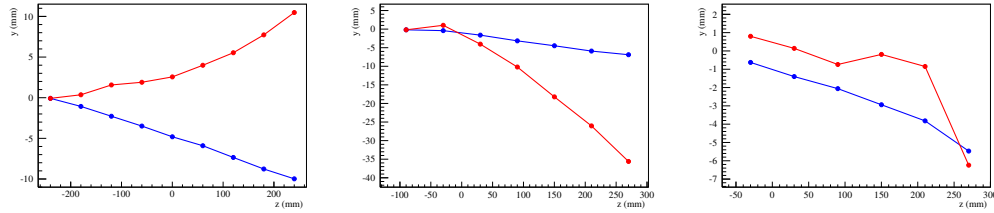


Fig. 5. Examples of events as recorded on the y - z view of the tracker. In the right panel an event in which the pair production occurs in an x -oriented layer is shown. Markers having the same color belong to the same particle. Only the tracking in the tracker/converter is reported.

ing coordinate resolution of 3 mm at 10 MeV, 0.5 mm at 100 MeV and 0.1 mm at 1 GeV.

Track reconstruction: a good reconstruction of the first two hits after interaction is important to guarantee the best estimation of the production directions of the particles. These are correctly identified with an efficiency better than 85% at 10 MeV, 92% at 100 MeV and better than 97% at 1 GeV.

The last two hits before the beginning of the magnetic field are crucial for the correct analysis of the momentum of each particle. The efficiency of this reconstruction is almost identical to that relative of the first hits of the tracks.

Finally for a successful track reconstruction each “head” of a track (from the vertex finding) needs to be linked to the correct “tail” (from the Hough Transform). The correct identification is achieved with an efficiency of 63% at 10 MeV, 73% at 100 MeV and 95% at 1 GeV.

Degeneracy removal: the recombination of x - z and y - z views, using the tilted layer, achieves different efficiencies with different rotation angles. In Figure 6, values found varying the angle from 0 to 45 degrees are shown. With no rotation there’s no criterion to resolve the degeneracy so the efficiency is, purely by chance, just one half. The efficiency improves with larger angles, reaching a stable value of about 83% above 7 degrees. Placing a sensor pair with large tilt angle at the end of the telescope stack may degrade the detector acceptance. A choice of a very small tilt angle, as for example 3° , would guarantee a recombination efficiency of about 80% with a negligible reduction of detection acceptance.

Overall reconstruction efficiency: the global reconstruction efficiency, taking into account all aforementioned effects, will be then 50% at 10 MeV, 69% at 100 MeV and 76% at 1 GeV.

Point Spread Function: the directions of the incident photons reconstructed for every simulated event will give the reconstructed Point Spread Function of the detector. The distribution obtained at different energies are illustrated in Figure 7. As expected, the distribution gets narrower as the energy increases. The 68% containment radius of these distribution can be compared with the data expected by the PANGU proposal paper. As shown in Figure 8, there’s a very good agreement between the results of the present study and the PANGU expectation, confirming the important improvement in terms of performance in the Sub-GeV region with respect to the Fermi-LAT angular resolution.

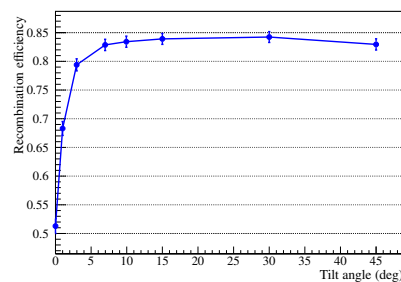


Fig. 6. Recombination efficiency as a function of the rotation angle of the tilted layer.

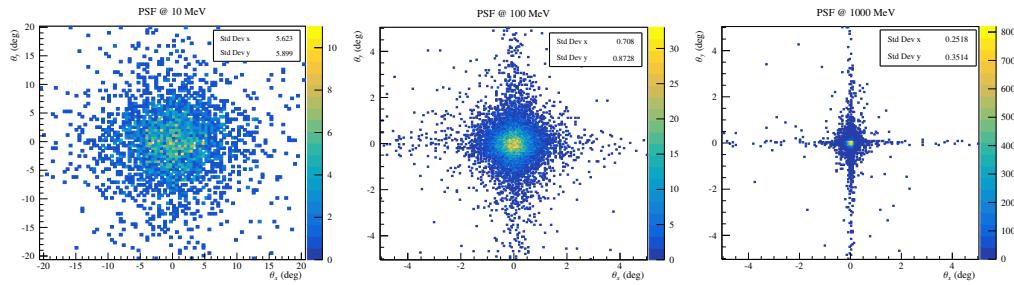


Fig. 7. Distribution of the reconstructed direction of monochromatic photons from a point-like source at three different energies at 10 MeV, 100 MeV and 1 GeV in the left, central and right panel respectively. These results are in the layout b) case.

6. Silicon tracker construction

Given the large effort, in terms of manpower, required to realize the silicon sensors, we decided to explore the synergy with another project having similar needs. Also the FOOT project [Valle et al. (2019)], indeed, needed silicon sensors with, essentially, the minimum possible thickness to keep very low the material budget, and opted to have the microstrip technology to keep under control the number of readout channels. We decided, thus, to share the effort and realize the needed silicon sensors as well as a new Data Acquisition, DAQ, system. The DAQ has been designed to be modular, compact and easily deployable even for a one night BT run. A typical BT conducted in an hospital or in general in a medical facility, indeed, is performed during the night, when there are no patients. Conducting BT's in this kind of facilities is crucial for the FOOT project. The possibility to conduct a BT with a photon beam for radio-therapy, in the same kind of facility, however, is a good added value for the POX project.

6.1. The microstrip silicon detectors

Each microstrip detector¹ has 640 (1920) strips with a 150 (50) μm readout (implant) pitch. Each sensor will measure an x or y coordinate via a 150 μm thick sensor with an active area of $96 \times 96 \text{ mm}^2$. The thickness has been chosen

¹ the sensors are produced by Hamamatsu Photonics

to be as minimum as possible, as suggested by the simulations, but enough to have a reasonable Signal-to-Noise ratio, S/N. Also the costs related to a too thin, and fragile, detector, have been taken into account.

As shown in Fig.9, each sensor is wire-bonded on a PCB, called “hybrid”. Each hybrid is read out by an ADC board. Finally the ADC board is connected to a DE10-Nano board that assembles the event and ships it to the main DAQ (i.e. the PC). The sensors and the Front End electronics will be hold by a light support structure designed not to add any additional material in the particle path. A hybrid board hosts one sensor and ten 64-channels, low-noise, and low-power IDE1140s Front-End chips². Each ADC board serves one x - y plane, i.e. two microstrip detectors, connected via two 40-pin connectors. The board embeds ten 12-bit AD7276A³ ADCs and each of them digitizes two IDE1140 outputs. The board also includes one device to generate the bias voltage for the x - y plane and the buffers/drivers for the DAQ board. The ADC board directly plugs to the DAQ board, i.e. a Terasic DE10-Nano board. This commercial board is the core unit of the x - y plane readout with an Intel Cyclone V System-On-Chip device that em-

² the commercial readout devices are produced by IDEAS, <https://ideas.no/products/ide1140>

³ the ADCs are produced by Analog Devices, <https://www.analog.com/en/products/ad7276.html>

beds an FPGA and a Microcontroller, referred to as Hard Processor System, HPS.

To maintain a cost-effective verification approach, $x - y$ modules are composed by two single-sided detectors with strips running in perpendicular directions, and held by a common custom support structure made of aluminum. In total 20 (10) single-sided detectors (supporting structures) have been built. Since the simulations show that the MCS effect seems better mitigated by adopting a layout with 20 equally-spaced sensors measuring the two views alternately, the implemented solution, useful for the tests and the commissioning of the sensors, will be substituted by a single sensor version of the mechanics.

The DAQ is very light, modular and compact, as show in Figure 10.

6.2. First experimental tests

The silicon tracker modules and its DAQ system have been designed and produced during 2020 and 2021. Given the COVID-19 pandemic situation, up to the mid of 2021, a test of the system with a BT has not been possible. On the other hand, sensors have been tested with cosmic ray muons in the labora-

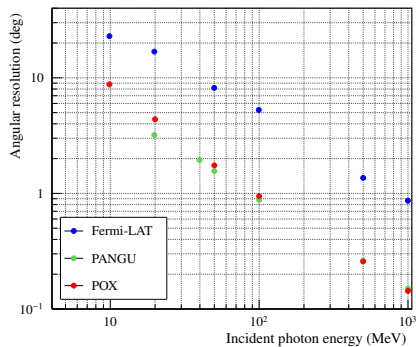


Fig. 8. Angular resolution (meant as the 68% containment radius of the PSF) obtained for the POX simulation as a function of the energy (red marks) compared to the performance expected according to the PANGU proposal paper (green marks, [Wu et al. (2014)]) and the actual resolution of the Fermi Large Area Telescope (in blue, [Ackermann et al. (2012)]).



Fig. 9. Single silicon sensor and its readout: from bottom to top the ADC board, the DE10-Nano board, and one hybrid board with ten IDE1140 FE ASIC's and one sensor.

tory (cfr. Figures 11 and 10) and with radioactive sources. From Figure 11 it is possible to see the performance of the sensors especially in terms of S/N: pedestal and signal are well separated. Cutting the clusters with a $S/N < 3.5$ (i.e. ~ 9 ADC channel units) we expect ~ 0.15 noisy clusters per sensor per event.

Unfortunately, spatial resolution has not been measured since a BT with charged particles is generally needed. The first possibility to test the sensors with a charged particles beam came only in the second half of 2021: the detectors have been exposed to low energies (Sub-GeV) ion beams at CNAO in Italy (Carbon nuclei) and GSI in Germany (Oxygen nuclei) in the context of FOOT BT's and to high energy (tens or hundreds of GeV) protons, muons and electrons beams at the PS and SPS facilities at CERN in Switzerland. The collected data are being analyzed and will per-

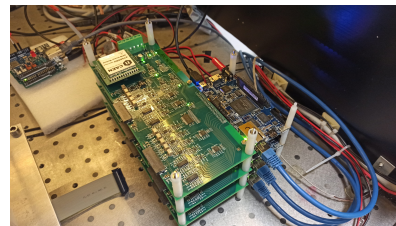


Fig. 10. A "stack" of three ADC and DE10-Nano boards, used to read out six silicon sensors for the cosmic ray tests in lab.

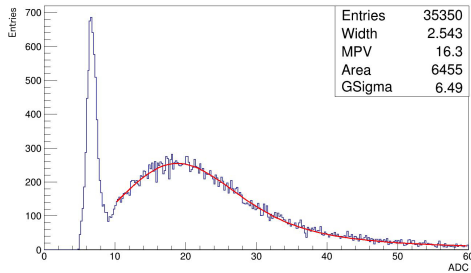


Fig. 11. Distribution of the signal (in ADC channel units) measured by a single silicon sensor exposed, in lab, to cosmic ray muons. The peak at lower values is coming from the noise contribution, while the fitted population on the right is the signal coming from the muons.

mit the test and commissioning of the sensors in a full tracking arrangement.

7. Planned experimental campaign

The campaign for the experimental verification of the PANGU approach will be conducted with the silicon sensors, described in Sec.6.1 and produced after the optimization phase of the project. The silicon sensor telescope shall be exposed to a Sub-GeV γ -ray beam, better if of known energy (i.e. *tagged*).

Given the limited world-wide availability of facilities with a tagged photon beam service and given the typical photon beam rate it is of primary importance, then, to design and prepare with great care the experimental campaign to maximize the result yield during the beam granted time. An optimization has been prepared for a beam test setup made of 20 tracking layers conceived as a preliminary test phase preceding the full characterization of a possible PANGU-like detector with a larger number of tracking sensors.

The design and preparation of the BT involved the optimization of the silicon sensor spacing, the effect of the air in the BT setup, of the spectrometric momentum resolution, and of the beam spot size and divergence, the computation of the needed statistics to measure the PSF, as function of the energy, with the required accuracy, and the optimization of the

beam electron “multiplicity” (cfr. [Cattaneo et al. (2012)]).

The natural choice for the facility to conduct the BT campaign is the INFN Beam Test Facility (BTF) in Frascati, where the AGILE [Tavani et al. (2009)] detector has been tested before launching it into space. An alternative option would be the Mainz Microtron, MAMI, where also polarized beams of photons are available [Lohmann et al. (1994)].

8. Conclusions

In this work we describe the studies conducted to verify the PANGU idea to investigate the gamma-ray Sub-GeV energy range.

A detailed MC simulation of the detector has been used to assess the optimal silicon sensor thickness for the instrument: this resulted to be around $150\mu\text{m}$, i.e. the thinnest thickness achievable not degrading too much the S/N of the sensor and without impacting significantly in the cost of the silicon wafer procurement and in the mechanical handling.

A dedicated reconstruction software has been developed in order to demonstrate the possibility to achieve the PANGU target angular resolution with realistic data. The preliminary expectations by the PANGU collaboration have been confirmed.

Twenty silicon sensor modules have been realized together with a new DAQ system designed to be compact, modular and easily deployable even for BT setups with limited spaces. A first experimental verification of produced sensors has been performed, using cosmic muons at ground, confirming a very good behaviour of the sensors in terms of S/N. In the second half of 2021 the detectors have been exposed to ion, proton, muon and electron beams at CNAO (Italy), GSI (Germany) and at the PS and SPS facilities at CERN (Switzerland). The collected data are being analyzed to assess the commissioning of the sensors in a full tracking arrangement.

The design and optimization of the experimental setup has been tailored for a BT to be conducted with a tagged photon beam at the BTF facility in Italy or at the MAMI facility

in Germany. This will be the first experimental verification of the PANGU detector performances.

Acknowledgements. We acknowledge financial contribution from the agreement ASI-INAF n.2017-14-H.0. This work has been supported as well by the Università degli Studi di Sassari with “Fondo di Ateneo per la ricerca 2019”. We also thank the FOOT colleagues, in particular L. Servoli (INFN Sez. Perugia), for sharing part of the effort in the design and construction of the microstrip silicon sensors and their DAQ.

References

- Ackermann, M., Ajello, M., Albert, A., et al. 2012, *The Astrophysical Journal Supplement Series*, 203, 4
- Agostinelli, S., Allison, J., Amako, K., et al. 2003, *Nuclear Instruments and Methods in Physics Research Section A: Accelerators, Spectrometers, Detectors and Associated Equipment*, 506, 250
- Alpat, B., Ambrosi, G., Azzarello, P., et al. 2010, *Nuclear Instruments and Methods in Physics Research Section A: Accelerators, Spectrometers, Detectors and Associated Equipment*, 613, 207
- Atwood, W. B., Abdo, A. A., Ackermann, M., et al. 2009, *The Astrophysical Journal*, 697, 1071
- Azzarello, P., Ambrosi, G., Asfandiyarov, R., et al. 2016, *Nuclear Instruments and Methods in Physics Research Section A: Accelerators, Spectrometers, Detectors and Associated Equipment*, 831, 378, proceedings of the 10th International “Hiroshima” Symposium on the Development and Application of Semiconductor Tracking Detectors
- Bernard, D., Bruel, P., Frotin, M., et al. 2014, in *Space Telescopes and Instrumentation 2014: Ultraviolet to Gamma Ray*, ed. T. Takahashi, J.-W. A. den Herder, & M. Bautz, Vol. 9144, International Society for Optics and Photonics (SPIE)
- Bigongiari, G., Adriani, O., Albergo, S., et al. 2019, *Universe*, 5
- Bykov, A., Gehrels, N., Krawczynski, H., & al. 2012, *Space Science Reviews*, 173, 309
- Cattaneo, P., Argan, A., Boffelli, F., et al. 2012, *Nuclear Instruments and Methods in Physics Research Section A: Accelerators, Spectrometers, Detectors and Associated Equipment*, 674, 55
- Chang, J., Ambrosi, G., An, Q., et al. 2017, *Astroparticle Physics*, 95, 6
- Dong, Y., Quan, Z., Wang, J., et al. 2016, in *Space Telescopes and Instrumentation 2016: Ultraviolet to Gamma Ray*, ed. J.-W. A. den Herder, T. Takahashi, & M. Bautz, Vol. 9905, International Society for Optics and Photonics (SPIE), 1861 – 1868
- Duda, R. & Hart, P. 1972, *Comm. ACM*, 15-1, 11
- D'Urso, D. 2017, POX - Pangu Optimization and eXperimental verification, <https://1.infn.it/asi-pox> - Studi per future missioni scientifiche (Accordo Attuativo ASI-INAF n.2017-14-H.0)
- Funk, S. 2015, *Annual Review of Nuclear and Particle Science*, 65, 245
- Hunter, S. D., Bloser, P. F., Depaola, G. O., et al. 2014, *Astroparticle Physics*, 59, 18
- Kanbach, G., Andritschke, R., Zoglauer, A., et al. 2005, *Nuclear Instruments and Methods in Physics Research A*, 541, 310
- Lebrun, F., Aharonian, F., Beckmann, V., et al. 2010, in *8th INTEGRAL Workshop on the Restless Gamma-Ray Universe*, INTEGRAL 2010, ed. P. of Science
- Lohmann, D. et al. 1994, *Nucl. Instrum. Meth. A*, 343, 494
- Mori, N. 2021, *Nuclear Instruments and Methods in Physics Research Section A: Accelerators, Spectrometers, Detectors and Associated Equipment*, 1002, 165298
- Morselli, A., Argan, A., Barbiellini, G., et al. 2013, in *Nuclear Physics B - Proceedings Supplements. Proceedings of the 9th workshop on Science with the New Generation of High Energy Gamma-ray Experiments: From high energy gamma sources to cosmic rays, one century after their discovery*, ed. I. D. Mitri, N. Giglietto, G. Marsella, & A. Surdo, Vol. 239-240, ScienceDirect, 193–198
- Mårtensson, M. & the ATLAS Collaboration. 2016, in *The 25th International workshop on vertex detectors, Vertex 2016*, ed.

- P. of Science
- O'Neill, T., Akyüz, A., Bhattacharya, D., Samimi, M. P. J., & Zych, A. 2001, in *GAMMA 2001: Gamma-Ray Astrophysics 2001*. AIP Conference Proceedings, Vol. 587, 882–886
- Pendleton, G., Binns, W., Israel, M., et al. 1999, in *EUV, X-Ray, and Gamma-Ray Instrumentation for Astronomy X*, ed. O. Siegmund & K. Flanagan, Vol. 3765, International Society for Optics and Photonics (SPIE), 12–21
- Pendleton, G., Fishman, G., Parnell, T., et al. 1996, in *Gamma-Ray and Cosmic-Ray Detectors, Techniques, and Missions*, ed. B. Ramsey & T. Parnell, Vol. 2806, International Society for Optics and Photonics (SPIE), 164–174
- Rieger, F., de Ona-Wilhelmi, E., & Aharonian, F. 2013, *Frontiers of Physics*, 8, 714
- Tavani, M., Barbiellini, G., Argan, A., et al. 2009, *A&A*, 502, 995
- Valle, S., Alexandrov, A., Ambrosi, G., et al. 2019, *Perspectives in Science*, 12, 100415
- Wu, X., Su, M., Bravar, A., et al. 2014, in *Space Telescopes and Instrumentation 2014: Ultraviolet to Gamma Ray*, ed. T. Takahashi, J.-W. A. den Herder, & M. Bautz, Vol. 9144, International Society for Optics and Photonics (SPIE), 120 – 134